Optics & Laser Technology 181 (2025) 111723

Contents lists available at ScienceDirect

Optics and Laser Technology

journal homepage: www.elsevier.com/locate/optlastec

Full length article

Regulating thermal management by a $CsPbClBr_2$/Ag hybrid microcavity for stable room temperature blue lasing with low threshold

Shulei Li [a], Zhenxu Lin [b,d,*], Quantong Deng [a], Fu Deng [b], Mingcheng Panmai [c], Junying Chen [e,f], Yuheng Mao [b], Shimei Liu [b], Jun Dai [a], Yunbao Zheng [a], Rui Huang [d,*], Sheng Lan [b,*]

[a] School of Optoelectronic Engineering, Guangdong Polytechnic Normal University, Guangzhou 510665, China
[b] Guangdong Provincial Key Laboratory of Nanophotonic Functional Materials and Devices, School of Information and Optoelectronic Science and Engineering, South China Normal University, Guangzhou 510006, China
[c] School of Electrical and Electronic Engineering, Nanyang Technological University, Singapore 639798, Singapore
[d] School of Material Science and Engineering, Hanshan Normal University, Chaozhou 521041, China
[e] Institute of Quantum Physics, School of Physics, Central South University, Changsha 410083, China
[f] State Key Laboratory of Precision Manufacturing for Extreme Service Performance, Central South University, Changsha 410083, China

ARTICLE INFO

Keywords:
Perovskite
Supercrystal
Hybrid microcavity
Thermal accumulation
Stable perovskite laser

ABSTRACT

Realization of long-term stable lasing from all-inorganic perovskite supercrystals is highly desirable for practical applications in optoelectronic devices. However, lasing from perovskite supercrystals excited by continuous wave laser light remains a challenge due to the photoluminescence degradation induced by thermal accumulation. Here, we report highly stable lasing with low threshold fom a $CsPbClBr_2$ supercrystal placed on a thin Ag film, which form a $CsPbClBr_2$/Ag microcavity, by managing the thermal distribution inside the $CsPbClBr_2$ supercrystal. Combined numerical simulations and lifetime measurements, the localized electric field in such a hybrid microcavity leads to a spatially localized temperature distribution, which plays a crucial role in suppressing the thermal accumulation on the surface and in eliminating non-radiative recombination defects. The effective thermal management in the hybrid microcavity renders highly stable lasing with low threshold under the irradiation of continuouw wave laser light. Our findings provide a feasible and universal approach to the development of long-term stable perovskite laser.

1. Introduction

All-inorganic cesium lead halide perovskites ($CsPbX_3$, (X=Cl, Br, I)) supercrystals (SCs), which are formed by the self-assembly of $CsPbX_3$ quantum dots (QDs)[1–4], have attracted great interest due to their outstanding physical and chemical properties, such as superfluorescence (SF)[2,5,6], long-term stability[7], and high optical gain[8,9]. Recently, in order to overcome optical loss and bring about new functions, optical resonant nanostructures have been introduced and extensively studied over the last decade[10–12]. In particular, $CsPbX_3$ SCs with micrometer sizes can serve as optical microcavities supporting whispering gallery modes (WGMs) owing to their regular geometric morphologies and smooth surfaces[13–15]. For this reason, stimulated emission from $CsPbX_3$ SCs can be easily realized. For instance, room temperature nanosecond-sustained green lasing with a low threshold (~25 μJ/cm^2) was demonstrated very recently in $CsPbBr_3$ SCs[16]. However, one of the main obstacles that limits the lasing stability of mixed halide $CsPbX_3$ SCs is light-induced migration of halide anion mediated by defect states, which leads to the phase segregation[17–19]. In addition, the thermal accumulation on the surfaces of $CsPbX_3$ SCs usually causes local overheating under the irradiation of continuous wave laser light due to the low thermal conductivity of the perovskite (~0.4 W/m•K), leading to the degradation of the photoluminescence (PL) [20,21]. This surface thermal accumulation becomes more serious for $CsPbX_3$ SCs with micrometer sizes, dramatically degradating the emission efficiencies of $CsPbX_3$ SCs. So far, the lasing stability of $CsPbX_3$ SCs hinders the practical application in laser devices.

Organic ligands decorated on the surfaces of perovskite QDs, such as polymer compounds and oleic acid, can increase inter-particle spacing and prevent the aggregation of perovskite QDs, making them stable and

* Corresponding authors at: Guangdong Provincial Key Laboratory of Nanophotonic Functional Materials and Devices, School of Information and Optoelectronic Science and Engineering, South China Normal University, Guangzhou 510006, China (Z. Lin).
E-mail addresses: linzhenxu2013@163.com (Z. Lin), rhuang@hstc.edu.cn (R. Huang), slan@scnu.edu.cn (S. Lan).

https://doi.org/10.1016/j.optlastec.2024.111723
Received 17 May 2024; Received in revised form 31 July 2024; Accepted 27 August 2024

monodisperse in solution[22,23]. On the other hand, the interaction between the surface ligands of adjacent QDs can be exploited to realize the assembly of QDs. It has been demonstrated that $CsPbX_3$ SCs can be fabricated via polar solvent-assisted self-assembly of QDs by balancing the interaction force between solution–ligand and that between ligand–ligand[24–27]. In this case, the detachment of surface ligands induced by polar solvent will create dangling bonds on the surfaces of QDs. Such dangling bonds would induce local defects or structural distortions in $CsPbX_3$ SCs, which are responsible for the thermal-activated nonradiative processes and high Auger recombination losses for $CsPbX_3$ SCs under high excitation fluences[28–30]. The existence of such defects hampers the achievement of low-threshold lasing in $CsPbX_3$ SCs. In addition, $CsPbX_3$ SCs often suffer from significant compressive strain due to the soft nature of ligand shells on QDs, which is detrimental to the stability of SCs. Therefore, fabrication of high-quality $CsPbX_3$ SCs while suppression of laser-induced overheating is crucial for realizing stable lasing of $CsPbX_3$ SCs at room temperature.

Laser annealing is a common method used for eliminating the defects and residual strain in a crystal, including $CsPbX_3$ microplatelets[31–38]. Due to the low thermal conductivity of $CsPbX_3$, however, the thermal management in a $CsPbX_3$ SC during laser annealing is necessary in order to avoid the thermal accumulation on the surface of the $CsPbX_3$ SCs. Physically, the temperature distribution in a microcavity is strongly correlated with the electric field distribution in the microcavity, which determines the energy distribution of the irradiation laser light. It has been known that a hybrid nanocavity formed by a dielectric nanoparticle and a thin metal film can be employed to establish a spatially localized temperature distribution inside the nanocavity[32,39]. In addition, the thin metal film with a good thermal conductivity acts as a heat sink, effectively suppressing the thermal accumulation in the nanocavity[40–44]. Therefore, it is expected that the hybrid microcavity formed by a $CsPbX_3$ SC and a thin metal film can enhance the interaction of the $CsPbX_3$ SC with laser light and prevent the damage of $CsPbX_3$ SC from overheating. In this way, the long-term stability of $CsPbClBr_2$ SCs can be achieved under the irradiation of continuous wave laser light, which is crucial for realizing stable lasing at room temperature.

In this work, we investigated the thermal management in a hybrid microcavity formed by placing a $CsPbClBr_2$ SC on a thin silver (Ag) film. We found that the electric field distribution in the hybrid microcavity leads to a uniform temperature distribution in the $CsPbClBr_2$ SC, which is helpful for suppressing the thermal accumulation on the surface and reducing the non-radiative recombination of the defects. We demonstrated the stable lasing of the $CsPbClBr_2$/Ag with a low threshold under the excitation of continuous wave laser light at room temperature.

2. Materials and methods

2.1. Fabrication of $CsPbClBr_2$ QDs

In this work, $CsPbClBr_2$ QDs were synthesized by hot-injection method. Cesium carbonate (Cs_2CO_3, Aladdin, 99.99 %), lead(II) bromide ($PbBr_2$, Aladdin, 99.99 %), lead(II) chloride ($PbCl_2$, Aladdin, 99.99 %), oleic acid (OA, Aladdin, 90 %), oleyamine (OAm, Aladdin, 90 %), trioctylphosphine (TOP, Aladdin, 90 %) and octadecene (ODE, Aladdin, 95 %) were used as the reactant precursors. First, Cs-oleate precursors were fabricated according to a typical synthesis. 100 mg Cs_2CO_3, 1 mL OA were mixed with 10 mL ODE in a 100 mL three-neck flask. 138 mg $PbBr_2$, 103 mg $PbCl_2$, 2 ml TOP, 2 mL OA, and 2 mL OAm were mixed with 20 mL ODE in another 100 mL three-neck flask. Then, the above solutions were maintained at 90 °C for 30 min under vacuum in order to remove air and moisture and then heated to 120 °C for 60 min until the Cs-oleate/Pb-oleate is completely dissolved in ODE. After that, the temperature of Cs-oleate solution was kept at 120 °C under nitrogen atmosphere for further hot injection, while the temperature of Pb-oleate solution was gradually increased to 180 °C under nitrogen atmosphere and kept for 20 min. Subsequently, 2 mL hot Cs-oleate solution was swiftly injected into the Pb-oleate solution. After 5 s, the reaction mixture was immediately cooled down in an ice-water bath. The crude $CsPbClBr_2$ QDs solution was centrifuged at 9200 rpm for 5 min. The concentrated supernatan was dispersed with a mixture of hexane and acetone with a volume ratio of 1:1 and then centrifuged at 8800 rpm for 5 min. The final $CsPbClBr_2$ QDs supernatant was dissolved in the hexane solution.

2.2. Synthesis of $CsPbClBr_2$SC/Ag hybrid microcavities

The as-prepared 4 mL $CsPbClBr_2$ QDs solution added 4 ml methyl acetate was left standing at room temperature for ten days. Then 50 μL solution was spin-coated onto a 10*10 mm clean Ag/SiO_2 substrate at a rate of 4000 rpm for 30 s. The $CsPbClBr_2$ SC were form on the surface of Ag film. The 50-nm-thick Ag film used in this work was prepared on a SiO_2 substrate via thermal evaporation method, and the spatial distribution of Ag is uniform. After that, the substrates were dried in a vacuum oven for 12 h in ambient condition.

2.3. Characterization of $CsPbClBr_2$ QDs and $CsPbClBr_2$ SC/Ag hybrid microcavities

The morphology and component elements of $CsPbClBr_2$ SC were characterized by a scanning electron microscope (SEM) (Hitachi SU5000), a high-resolution transmission electron microscope (HR-TEM) (JEM-1400 PLUS) and energy dispersive spectroscopy (EDS) (Bruker EDS QUANTAX), respectively. The crystal structures of $CsPbClBr_2$ QDs and $CsPbClBr_2$ SC were characterized by X-ray diffraction (XRD) (Bruker D8 Advance) at 35 kV and 35 mA. The UV–Vis absorption spectra were measured by using a spectrophotometer (Shimadzu UV–Vis 3600).The PL spectra of $CsPbClBr_2$SC were collected by a 40 × UV objective lens in a Raman spectrometer system (Horiba LabRAM HR Evolution) equipped with a 325-nm He-Cd laser (Kimmon). The PL spectra of $CsPbClBr_2$ SC were collected by a 40 × UV objective lens in a Raman spectrometer system (Horiba LabRAM HR Evolution) equipped with a 325-nm He-Cd laser (Kimmon) and a long wave pass edge 325 nm-filter.

2.4. Optical characterization of $CsPbClBr_2$ SC/Ag hybrid microcavities

The 800 nm femtosecond laser light (Mira 900S, Coherent, 130 fs) was employed to excite $CsPbClBr_2$ SC, a high repetition rate 76 MHz was measure luminescence and power-dependent, and a low repetition rate of 3.8 MHz (obtained by using a pulse picker) and a time-correlated single photon system (lifespec II, Edinburgh Instruments) was employed to measure luminescence lifetimes. The single-mode lasing spectra measurement were performed by using 400 nm femtosecond pulses of 1 kHz (Legend, Coherent). A 325 nm CW laser was measured multimode lasing spectra. The laser light was focused on the samples by using the 50× objective lens (NA=0.8) of an inverted microscope (Axio Observer A1, Zeiss). The scattering light and photoluminescence were collected by using the same objective lens and directed to a spectrometer (SR-500i-B1, Andor) for analysis or to a coupled-charge device (DU970N, Andor) for recording.

2.5. Numerical simulation and analytical model

The scattering spectra of $CsPbClBr_2$ SC placed on a thin Ag film were calculated numerically by using the finite-difference time-domain (FDTD) method (FDTD solution, https://www.lumerical.com). In the numerical simulation, the side length of the $CsPbClBr_2$ SC is 2 × 2 μm and the height is 0.5 μm and is placed on the surface of Ag film. The dielectric constants of Ag was taken from the previous literature [45,46], and refraction index of $CsPbClBr_2$ SC were taken from the previous literature [47,48] with fitting the absorption peak in the measured spectra in our data. The dipole source was placed inside the $CsPbClBr_2$ SC to calculate the radiation intensity of the $CsPbClBr_2$/SiO_2

and $CsPbClBr_2$/Ag. In order to obtain converged simulation results, a perfectly matched layer boundary condition was employed to terminate the finite simulation region. The temperature distributions inside the hybrid microcavities were calculated numerically based on the finite element method (FEM) (COMSOL Multiphysics v5.6, https://www.comsol.com). The refractive index and thermal conductivity of $CsPbClBr_2$ SC were taken from literature[48–50].

3. Results and discussion

As shown in Fig. 1(a), we synthesized $CsPbClBr_2$ SCs with regular geometric shape by the self-assembly of monodispersed QDs assisted by polar solvent. The $CsPbClBr_2$ QDs were prepared by using typical high temperature hot injection following the procedures described in literature. Based on the transmission electron microscopy (TEM) image (Fig. 1(b)), the average size of the $CsPbClBr_2$ QDs was estimated to be $\sim 10 \pm 2$ nm. In addition, the distance between the lattice fringes of QDs was found to be $\sim$ 0.29 nm, corresponding to the (001) crystal plane of orthorhombic $CsPbClBr_2$[51]. This assignment was further confirmed by the X-ray diffraction (XRD) measurements shown in Fig. 1(c), where two double sharp peaks corresponding to the orthorhombic phase of $CsPbClBr_2$ are observed at $\sim 15.7°$ and ~ 31.4. In Fig. 1(d), we present the PL spectrum of $CsPbClBr_2$ QDs, which appears as a highly symmetric emission band at $\sim$ 478 nm with a full width at half maximum (FWHM) of $\sim$ 21 nm. All these characterizations indicate the high crystalline quality of the $CsPbClBr_2$ QDs used in the fabrication of $CsPbClBr_2$ SCs.

We also examined the crystal structures, morphologies and optical properties of the synthesized $CsPbClBr_2$ SCs. As shown in Fig. 1(c), the XRD spectrum of the $CsPbClBr_2$ SCs remains unchanged as compared with that of the $CsPbClBr_2$ QDs. The morphologies of the $CsPbClBr_2$ SCs were characterized by using scanning electron microscopy (SEM). The SEM image of a typical Fig. 1(e). It can be seen that the $CsPbClBr_2$ SC

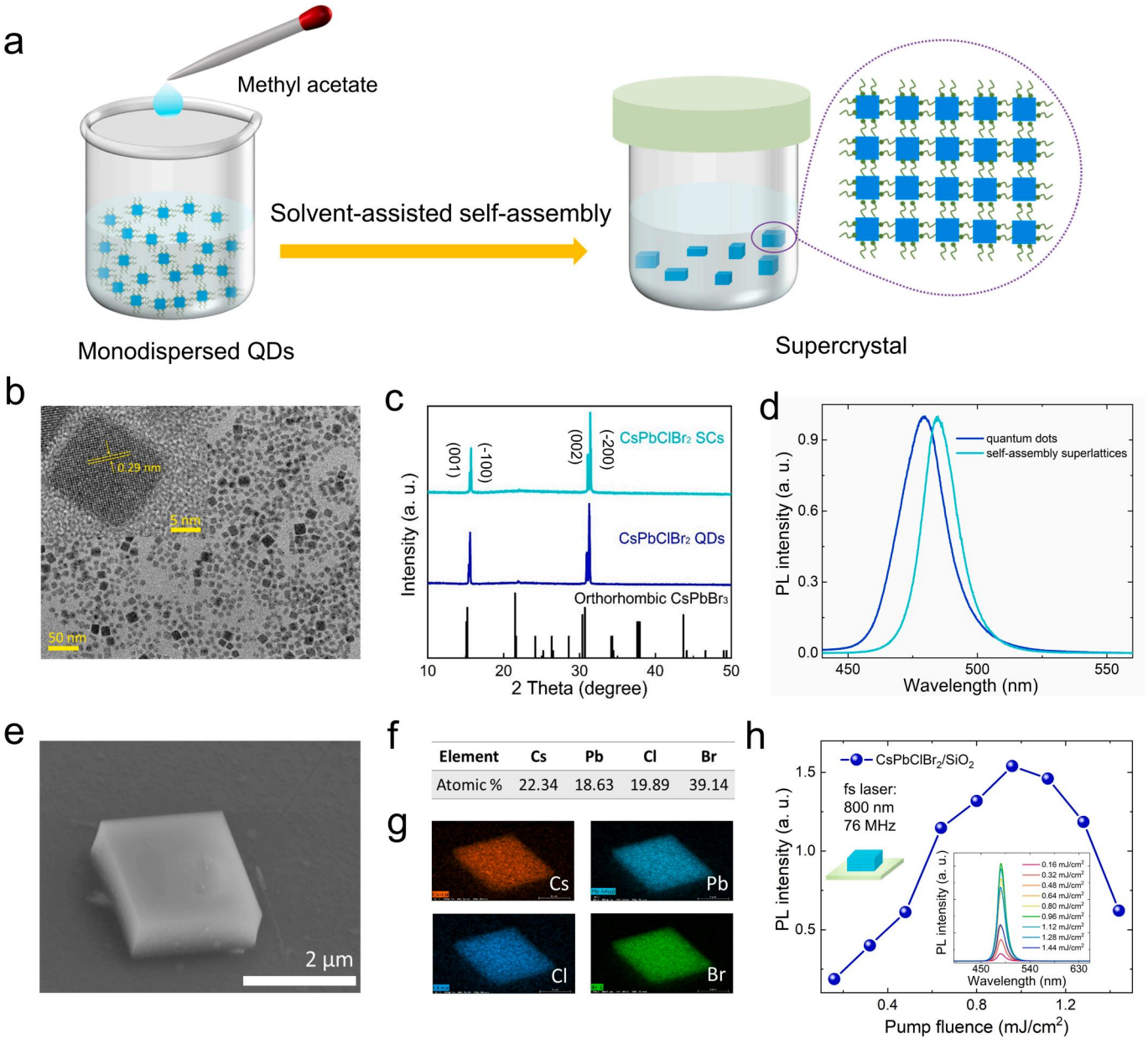

Fig. 1. (a) Schematics of the fabrication process of $CsPbClBr_2$ SC. (b)TEM image of the pristine $CsPbClBr_2$ SC. (c) XRD patterns of the $CsPbClBr_2$ SC, $CsPbClBr_2$ QDs, and reference peak of the $CsPbBr_3$. (d) The PL spectra of $CsPbClBr_2$ QDs and $CsPbClBr_2$ SC. (e) SEM image of a $CsPbClBr_2$ SC on an Ag film surface (f, g) EDS analysis of Cs, Pb, Cl, Br. (h) PL spectra measured for a $CsPbClBr_2$ supercrystal placed on the SiO_2 substrate excited by using 800 nm femtosecond laser pulses of 76 MHz at different pump fluence.

appears as a cuboid with a flat and smooth surface. The elemental analysis and mapping based on energy dispersive spectroscopy (EDS) are shown in Fig. 1(f) and (g), verifying the uniform distributions of elements (Cs, Pb, Cl, and Br) in the $CsPbClBr_2$ SC. The atomic ratio of Cs/Pb/Cl/Br = 1:1:1:2 is in good agreement with the stoichiometric ratio of $CsPbClBr_2$. Moreover, the PL spectrum of the $CsPbClBr_2$ SC is different from that of $CsPbClBr_2$ QDs, as shown in Fig. 1(d). A redshift of the PL peak (from ~ 478 to ~ 485 nm) and a narrowing of the FWHM (from ~ 21 to ~ 14 nm) is observed for the $CsPbClBr_2$ SC. This change in the PL spectrum is attributed to the formation of miniband in the $CsPbClBr_2$ SC due to the electronic coupling of neighboring QDs[52]. Remarkably, the emission from the $CsPbClBr_2$ SC remains stable for more than 30 min under the excitation of 325-nm continuous wave (CW) laser light with a power density of P=44.71 W/cm^2. This behavior is in contrast to the PL degradation observed for the QDs after only 3 min under the same excitation condition. Moreover, no halide phase segregation was observed for the $CsPbClBr_2$ SC. It indicates the remarkably improved photo-stability in the SC formed by the assembly of QDs, as reported in a previous study[53]. This suppression of halide phase separation is attributed to the reduction of exciton-phonon coupling and lattice strain resulting from the enhanced excitonic delocalization in the $CsPbClBr_2$ SC. Therefore, assembled superstructures with new properties generated by electronic coupling between QDs are expected to be applied in perovskite laser devices.

In fact, local defects and/or structural distortions are inevitably introduced in the fabrication process of $CsPbClBr_2$ SCs due to the detachment of surface ligands or large lattice mismatch. Although the photo-stability of $CsPbClBr_2$ SCs can be significantly improved as compared with QDs, PL degradation still occurs in a $CsPbClBr_2$ SC excited by using a high power density. In Fig. 1(h), we show the evolution of the PL intensity with increasing laser pump fluence observed for a $CsPbClBr_2$ SC placed on a SiO_2 substrate by using 800-nm femtosecond laser pulses of 76 MHz. A rapid PL quenching is clearly observed for laser fluence larger than 0.96 mJ/cm^2. Due to the low thermal conductivity of the perovskite, the local overheating induced by laser irradiation in the $CsPbClBr_2$ SC may lead to the aggregation of QDs, increasing surface defects and quenching the PL.

The recent results suggest that perovskites SC can be empowered by optical resonances, and the tight confinement of the electromagnetic field within it can promote light-matter interactions and control light emission at the wavelength of the material emission[6,12,53]. For the hybrid microcavity created by placing a $CsPbClBr_2$ SC on a thin Ag film, it is necessary to identify the optical modes supported by the hybrid microcavity, which can be employed to enhance the linear and nonlinear optical responses of the $CsPbClBr_2$ SC. In Fig. 2(a), we show the absorption and PL spectra of the $CsPbClBr_2$ SC. It was found that absorption and PL peaks of the $CsPbClBr_2$ SC was located at 492 nm. The refraction index of $CsPbClBr_2$ SC was taken from the previous literature [47,48] with fitting the absorption peak in the measured spectra in our data (see Fig. 2(b)). In Fig. 2(c), we show the radiation spectra of two $CsPbClBr_2$ SCs placed on an Ag/SiO_2 substrate and a SiO_2 substrate, respectively. In each case, a dipole source placed at the center of the

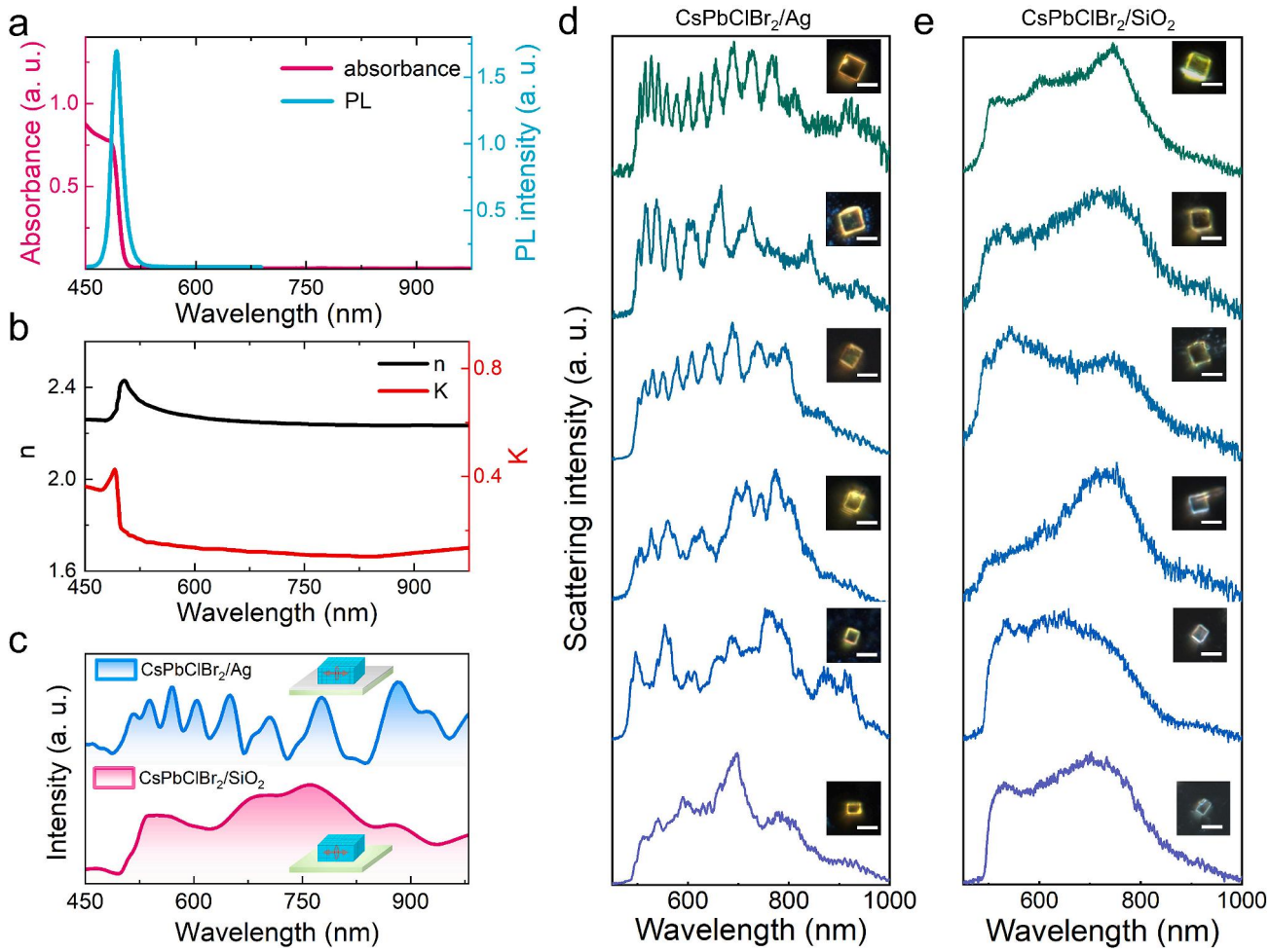

Fig. 2. (a) The absorption and PL spectra of $CsPbClBr_2$ SC. (b) The refraction index of CsPbClBr2 SC. (c) Radiation spectra calculated for a $CsPbClBr_2$ SC placed on the Ag/SiO_2 and SiO_2 substrates, respectively. The side length and thickness of the cuboidal SC are assumed to be 2 μm and 0.5 μm. Scattering spectra measured for $CsPbClBr_2$ SCs with different sizes placed on an Ag/SiO_2 substrate (d) and a SiO_2 substrate (e). Scale bar: 2 μm.

$CsPbClBr_2$ SC was used as the excitation source. It noticed that the $CsPbClBr_2$ SC placed on the Ag/SiO_2 substrate supports a variety of optical modes with high quality (Q) factors. In comparison, very few optical modes with large Q factors are observed in the $CsPbClBr_2$ SC placed on the SiO_2 substrate. For the hybrid microcavity composed of the $CsPbClBr_2$ SC and the Ag film, the high-Q optical modes may originate from the coherent interaction between the high-order Mie resonances and the whispering gallery modes (WGM) or Fabry-Perot (F-P) resonances. They are beneficial for the light amplification in the $CsPbClBr_2$/Ag hybrid microcavity. In order to gain a deep insight into the optical modes supported by $CsPbClBr_2$/Ag hybrid microcavities, we measured the scattering spectra of $CsPbClBr_2$/Ag hybrid microcavities with different sizes by using polarized white light and analyzer with cross polarization, as shown in Fig. 2(d). The scattering spectra measured for $CsPbClBr_2$ SCs placed on the SiO_2 substrate are also provided for comparison (see Fig. 2(e)). One can identify high-Q optical modes at the emission wavelength of $CsPbClBr_2$, especially for hybrid microcavities with large sizes. In comparison, very few optical modes with high Q factors are revealed in the $CsPbClBr_2$ SCs placed on the SiO_2 substrate. The Q value of most of the measured resonance mode is close

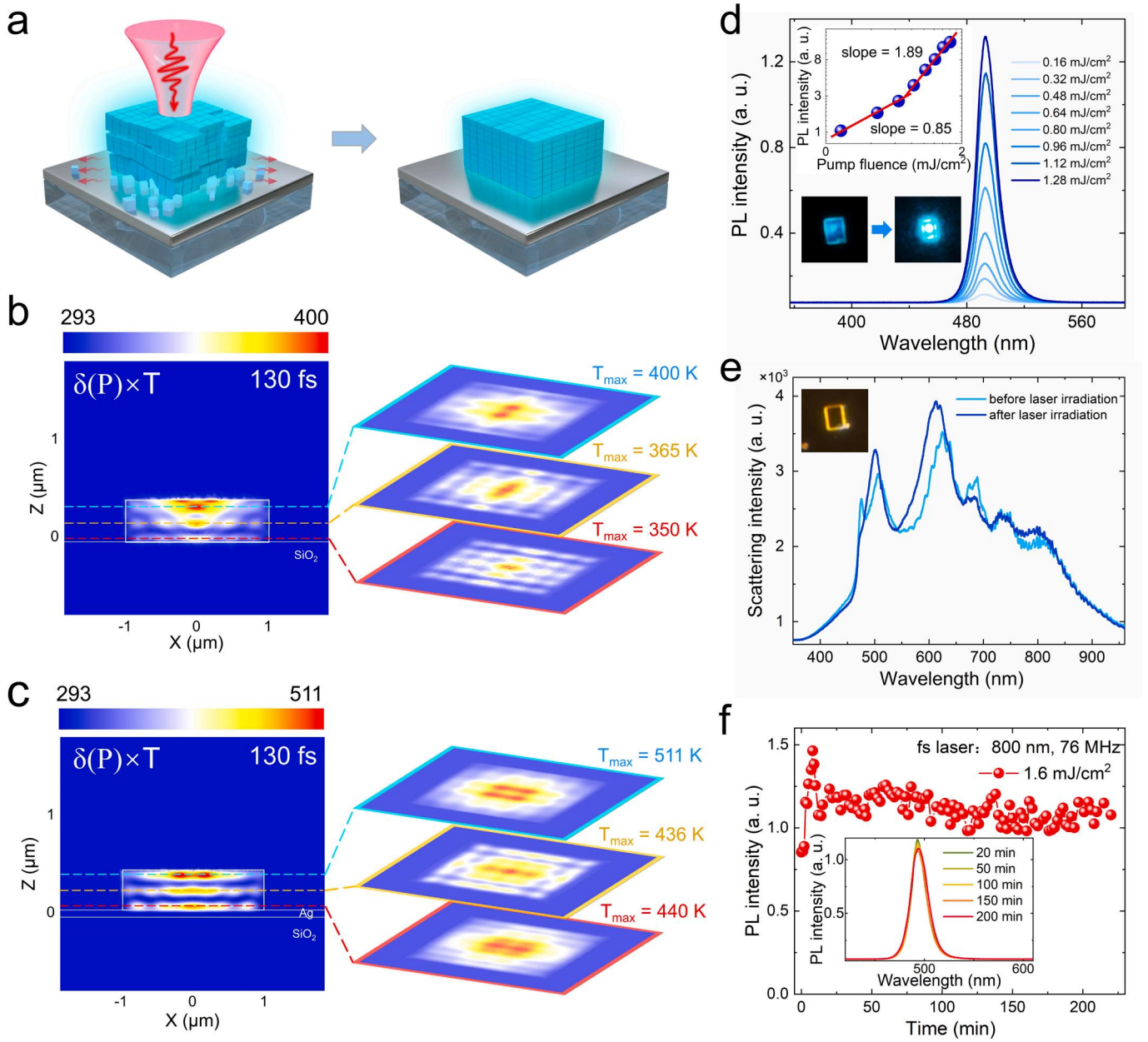

Fig. 3. (a) Schematic showing the annealing of a $CsPbClBr_2$ SC placed on an Ag/SiO_2 substrate induced by laser irradiation. (b) Transient temperature distribution in the XZ and XY planes (t = 130 fs) calculated for a $CsPbClBr_2$ SC placed on a SiO_2 substrate and excited by using a single 800-nm femtosecond laser pulse with a duration of 130 fs. (c) Transient temperature distribution in the XZ and XY planes (t = 130 fs) calculated for a $CsPbClBr_2$ SC placed on an Ag/SiO_2 substrate and excited by using a single 800-nm femtosecond laser pulse with a duration of 130 fs. (d) PL spectra measured for a $CsPbClBr_2$/Ag hybrid microcavity excited by using 800- nm femtosecond laser pulses at different pumping fluences. The dependence of the PL intensity on the pumping fluence plotted in a logarithmic coordinate and the optical image of the $CsPbClBr_2$ SC recorded by using a CCD at different pumping fluences are provided in the insets. (e) Forward scattering spectra measured for the $CsPbClBr_2$/Ag hybrid microcavity before and after the laser irradiation. The optical image of the $CsPbClBr_2$ SC recorded by using a CCD is shown in the inset. (f) PL intensities of the $CsPbClBr_2$/Ag hybrid microcavity excited continuously by using 800-nm femtosecond laser pulses. The PL spectra recorded at different times are shown in the inset.

to the simulation, and only some resonance mode has lower Q value. This is mainly because compared with the simulation model, the synthesized $CsPbClBr_2$ SC edge has a certain curvature, which is not so sharp.

As demonstrated above, the optical modes supported by a $CsPbClBr_2$/Ag hybrid microcavity possess electric field distributions similar to standing waves inside the $CsPbClBr_2$ SC. At the excitation wavelength, such a localized electric field distribution leads to a spatially-localized temperature distribution, which is helpful for eliminating the defects induced in the $CsPbClBr_2$ SC during the self-assembly process, as schematically illustrated in Fig. 3(a). As a result, the $CsPbClBr_2$/Ag hybrid microcavity is expected to exhibit improved stability under the excitation of laser light. In order to find out the effect of the Ag film on the temperature distribution in a $CsPbClBr_2$ SC, we employed numerical simulation to calculate the temperature change induced in a $CsPbClBr_2$ SC placed on a SiO_2 substrate by a single 800-nm femtosecond laser pulse with a duration of 130 fs, as shown in Fig. 3(b). The simulation is based on the two temperature model with considering the pulse duration of the pulse and it is widely used in nanophotonic system under femtosecond laser excitation[54–56]. It should be noted that the model is based on a linear model rather than the nonlinear effect such as two/multi-photon absorption for simplicity, which is enough for explaining the laser heating effect on the sample[57,58]. It is found that the temperature rise is not uniform in the SC and it primarily occurs at the top of the SC. This behavior implies that overheating may appears on the surface of the SC, leading to the increase of surface defects. The temperature is gradually transmitted from the top to the bottom, and gradually decreases, only a small region of the $CsPbClBr_2$ SC is affected by laser heat. This prediction is supported by the PL lifetime measured for the $CsPbClBr_2$ SC placed on a SiO_2 substrate under continuous laser irradiation (see Fig. 4(a)). In this case, a gradual decrease of the PL lifetime is observed with increasing irradiation time, indicating an increase of nonradiative decay rate. This explains the rapid PL quenching observed for $CsPbClBr_2$ SCs placed on a SiO_2 substrate at high excitation power densities. Therefore, the thermal management in a $CsPbClBr_2$ SC plays a crucial role in improving the photo-stability of the $CsPbClBr_2$ SC.

In Fig. 3(c), we show the temperature change induced in a $CsPbClBr_2$/Ag hybrid microcavity under the same excitation condition. It is noticed that the temperature rise in the $CsPbClBr_2$ SC no longer contracts at the top of the SC. Instead, it is uniformly distributed at the top, in the middle and at the bottom of the SC. This modification in the temperature distribution induced by the addition of the Ag film greatly suppresses the overheating appearing on the surface of the SC under laser irradiation. The temperature of $CsPbClBr_2$ SC placed on Ag film after laser action is higher than that placed on SiO_2 substrates. Surprisingly, the temperature at the bottom of $CsPbClBr_2$ SC is actually higher than that in the central region, and the distribution of the high-temperature region is larger, which is caused by the field localization of plasmon at the gap position of $CsPbClBr_2$ SC and Ag film. This main that more areas are affected by the laser annealing. On the other hand, it is helpful for eliminating the defects induced in the SC during the self-assembly process by exploiting the laser-induced annealing. In order to confirm this suspect, we monitored the PL lifetime of a $CsPbClBr_2$ SC, as shown in Fig. 4(b). A gradual increase in the PL filetime is observed with increasing irradiation time, implying the decrease of nonradioactive recombination centers upon the laser irradiation[59]. This behavior indicates the possibility for realizing ultra-stable light emission from a $CsPbClBr_2$ SC/Ag hybrid microcavity under continuous laser irradiation.

We examined the PL spectra of a $CsPbClBr_2$ SC/Ag hybrid microcavity by using 800-nm femtosecond laser pulses at different pumping fluences (p), as shown in Fig. 3(d). The dependence of the PL intensity on the pumping fluence plotted in a logarithmic coordinate is provided in the inset. At low pumping fluences, the slope extracted from the dependence of the PL intensity on the pumping fluence (~0.82) is smaller than the expected value for two-photon-induced luminescence (TPL) (~2.0). A slope of ~ 2.0 is observed at high pumping fluences, indicating the TPL nature of the emission from the hybrid microcavity. The increase of the slope from ~ 0.82 to ~ 2.0 is mainly caused by the elimination of the defects inside the $CsPbClBr_2$ SC induced by laser annealing. Interestingly, the blue light emission from the centers of four edges can be clearly observed and is considered to result from the WGM modified emission. In order to confirm the effect of laser annealing, we examined the scattering spectra of the $CsPbClBr_2$/Ag hybrid microcavity before and after the laser irradiation by using dark-field microscopy, as shown in Fig. 3(e). The optical image of the $CsPbClBr_2$ SC recorded by using a charge coupled device (CCD) is shown in the inset. Surprisingly, we observed increased intensities and blue shifts for the main scattering peaks. It implies that the local defects or structural distortions in the $CsPbClBr_2$ SC are removed by the temperature rise induced by laser irradiation. As a result, the emission from the $CsPbClBr_2$ SC becomes more efficient and stable. In Fig. 3(f), we show the PL intensities of the $CsPbClBr_2$/Ag hybrid microcavity irradiated continuously by using 800-nm femtosecond laser pulses of 76 MHz at a pumping fluence of 1.6 mJ/cm^2. It can be seen that the PL intensity remained stable for more than

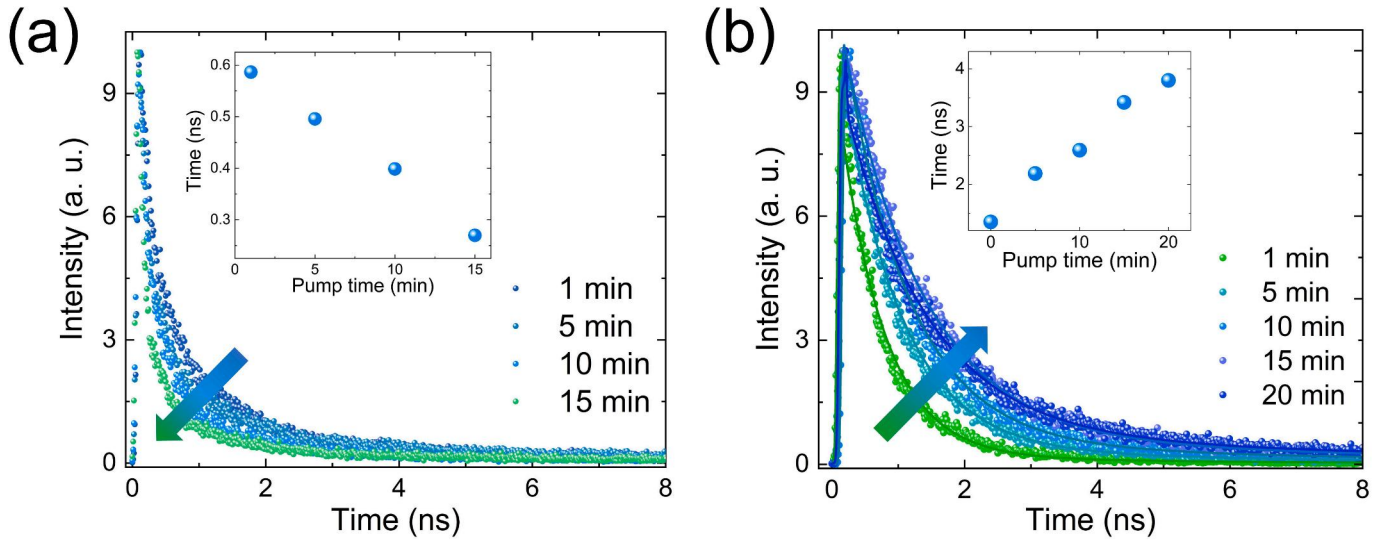

Fig. 4. (a) Pump fluence time-dependent PL decay of $CsPbClBr_2$ SC place on the SiO_2 substrate at room temperature by using the 800-nm femtosecond laser pulses of 3.8 MHz. (b) Pump fluence time-dependent PL decay of $CsPbClBr_2$ SC place on the Ag film by using the 800-nm femtosecond laser pulses of 3.8 MHz.

260 min.

At present, the major obstacle for realizing CW-laser-pumped perovskite lasers at room temperature is the thermal accumulation effect induced by CW laser light. As demonstrated above, the hybrid microcavity composed of a $CsPbClBr_2$ SC and a thin Ag film can effectively suppress the local overheating induced by laser irradiation. Therefore, it is expected that the stimulated emission from such a hybrid microcavity can be achieved under the excitation of CW laser light. In Fig. 5(a), we show PL spectra measured for a $CsPbClBr_2$ /Ag hybrid microcavity at different power densities by using 325-nm CW laser light. One can identify optical modes with narrow linewidths supported by the $CsPbClBr_2$ SC in the PL spectra. The dependence of the integrated PL intensity and the linewidth (FWHM) on the excitation power density is plotted in Fig. 5(b). It is noticed that the PL intensity increases rapidly when power exceeds a critical value (P~10 W/cm^2), where a transition from sublinear to superlinear behavior is observed. When the pump density was further increased, the narrow linewidth peaks dominated the emission spectrum and the output intensity increases dramatically, as shown in the inset of Fig. 5(b). Due to the coupling between the PL spectra of $CsPbClBr_2$ excitons and the WGM supported by $CsPbClBr_2$/Ag hybrid microcavity, the PL spectra acquired by the hybrid microcavity system shows a narrow linewidth resonance mode. However, the WGM supported by $CsPbClBr_2$/Ag hybrid microcavity has a high Q factor (as shown in Fig. 2(d)), its PL spectra is not much different from the FWHM of laser, and it is difficult to observe the obvious linewidth narrowing phenomenon at the threshold. In addition, it is found that the linewidth (FWHM) of the sharp optical mode appearing at ~ 498 nm is reduced to ~ 1.0 nm when the excitation power density is raised to P=44.71 W/cm^2, as shown in the inset of Fig. 5(b). The rapid increase in the PL intensity and the dramatic narrowing of the linewidth above the threshold indicates clearly the multi-mode lasing realized in the $CsPbClBr_2$/Ag hybrid microcavity. To further evaluate the superiority of the $CsPbClBr_2$/Ag hybrid microcavity, we tested amplified spontaneous emission (ASE) property by using 400-nm femtosecond laser pumping (130 fs, 1 kHz) at ambient conditions. In Fig. 5(c), we present power-dependent PL spectra of the $CsPbClBr_2$/Ag hybrid microcavity at different power densities. It is found that under low power densities (<36 μJ/cm^2), the intensity of photoemission increased slowly and the PL spectra can see a broad emission band (FWHM~26.3 nm) centered at ~ 490 nm. Strikingly, with the excitation power density is increased to ~ 54 μJ/cm^2, a sharp peak with a narrow linewidth (FWHM~5.4 nm) emerges at the low-energy shoulder of the emission band (~498 nm), as shown in Fig. 5(d). The nonlinear response of the light emission intensity and the dramatic narrowing in the linewidth to pump fluence confirms the ASE behaviors in the $CsPbClBr_2$/Ag hybrid microcavity.

An essential characteristic of optical gain materials is their photostability under laser irradiation. In order to examine the stability of the stimulated emission from the $CsPbClBr_2$/Ag hybrid microcavity by using 400-nm femtosecond laser pulse (130 fs, 1 kHz), the PL spectra recorded at different times are shown in Fig. 6(a). We monitored the peak intensity of the stimulated emission for more than 60 min, as shown in Fig. 6(b). It can be seen that the PL intensity remains stable for a long

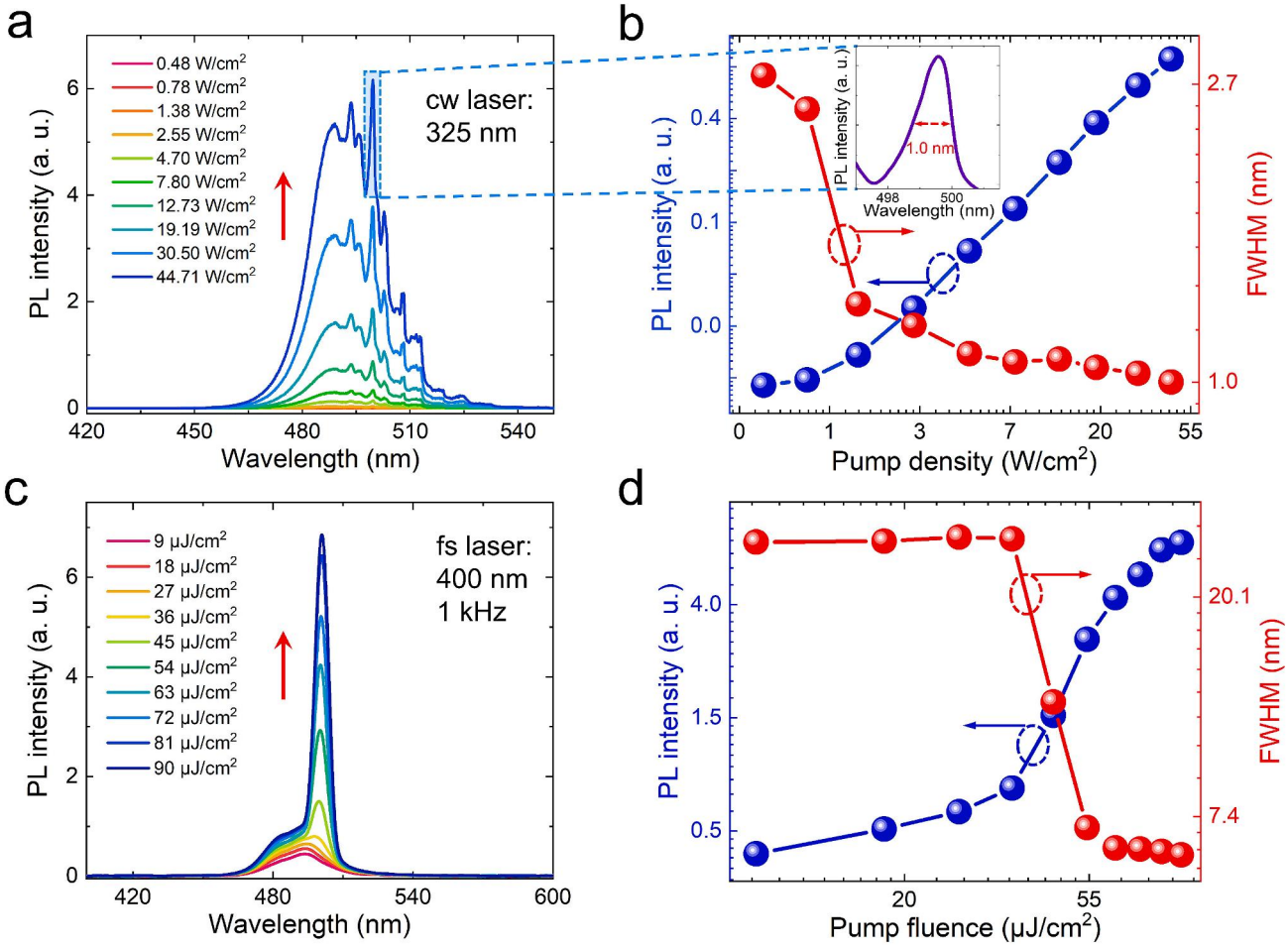

Fig. 5. (a) PL spectra measured for a $CsPbClBr_2$/Ag hybrid microcavity at different excitation power densities by using 325-nm CW laser light. (b) Dependence of the integrated PL intensity and linewidth on the excitation power density. The inset shows the magnified PL spectrum of a sharp optical mode with a narrow linewidth. (c) PL spectra measured for a $CsPbClBr_2$/Ag hybrid microcavity at different excitation power densities by using 400-nm femtosecond laser pulses. (d) Evolutions of the PL intensity and linewidth with increasing power density.

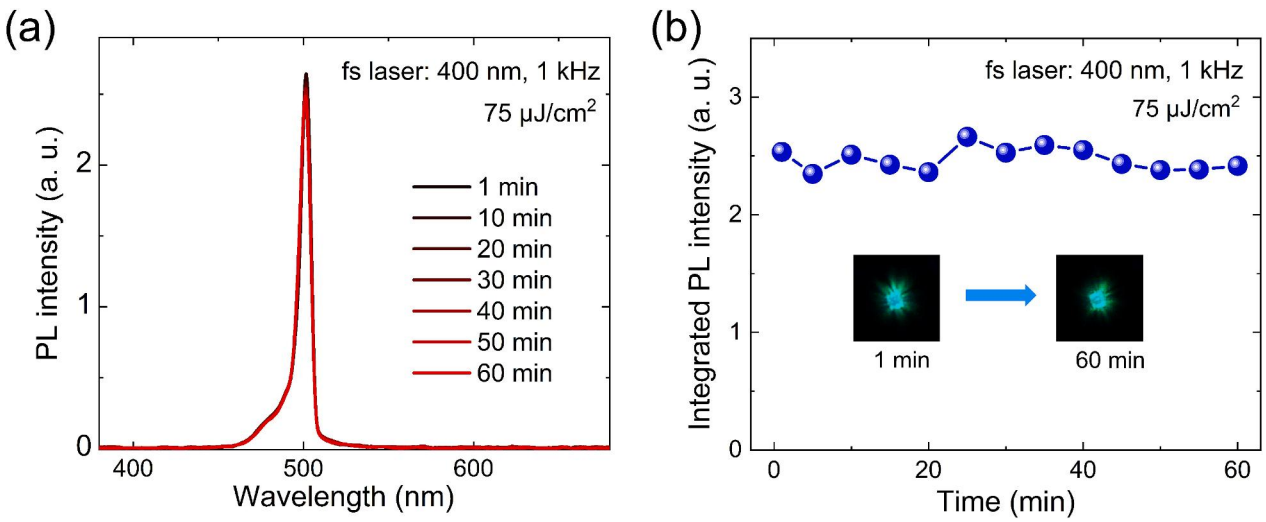

Fig. 6. (a) PL spectrum measured for the $CsPbClBr_2$/Ag hybrid microcavity at different times under the excitation of 400-nm femtosecond laser pulses. (b) Integrated PL intensities of the $CsPbClBr_2$/Ag hybrid microcavity recorded at different times under the excitation of 400-nm femtosecond laser pulses. The optical image of the $CsPbClBr_2$ SC recorded by using a CCD at 1 min and 60 min respectively are shown in the inset.

time under the continuous excitation of 400-nm femtosecond laser pulses. This feature indicates the great potential of $CsPbClBr_2$/Ag hybrid microcavities in making multimode lasers with low threshold and high stability.

4. Conclusions

In summary, we developed a method to manage the temperature distribution inside a $CsPbClBr_2$ SC creating a $CsPbClBr_2$/Ag hybrid microcavity. The strongly localized electric field achieved in the hybrid microcavity leads to relatively uniform temperature distribution inside the $CsPbClBr_2$ SC, which suppresses the thermal accumulation on the surface of the $CsPbClBr_2$ SC and reduces the non-radiative recombination centers inside the $CsPbClBr_2$ SC. We demonstrated multimode lasing in such a $CsPbClBr_2$/Ag hybrid microcavity at room temperature under the excitation of 325-nm CW laser light. Moreover, we showed ultra-stable emission from the $CsPbClBr_2$/Ag hybrid microcavity under the continuous excitation of 400-nm femtosecond laser pulses. Our findings indicate the great potential of such hybrid microcavities in making CW-light-pumped perovskite lasers with low threshold and high stability.

Funding.

This work was financially supported by the National Natural Science Foundation of China (Grant Nos. 12174123, 12374347), Guangdong Basic and Applied Basic Research Foundation (Grant No. 2022A1515010747), Start-Up Funding of Guangdong Polytechnic Normal University (2022SDKYA007), Project of Guangdong Province Key Discipline Scientific Research Level Improvement (2021ZDJS039), Project of Educational Commission of Guangdong Province of China (2019KTSCX096).

CRediT authorship contribution statement

Shulei Li: Writing – original draft, Validation, Investigation, Funding acquisition, Formal analysis, Data curation. **Zhenxu Lin:** Writing – original draft, Validation, Methodology, Formal analysis, Data curation. **Quantong Deng:** Investigation. **Fu Deng:** Formal analysis. **Mingcheng Panmai:** Formal analysis. **Junying Chen:** Formal analysis. **Yuheng Mao:** Formal analysis. **Shimei Liu:** Data curation. **Jun Dai:** Data curation. **Yunbao Zheng:** Investigation. **Rui Huang:** Supervision, Investigation, Funding acquisition. **Sheng Lan:** Writing – review & editing, Resources, Project administration, Methodology, Funding acquisition, Formal analysis.

Declaration of competing interest

The authors declare that they have no known competing financial interests or personal relationships that could have appeared to influence the work reported in this paper.

Data availability

No data was used for the research described in the article.

References

[1] Q. Wang, J. Tan, Q. Jie, H. Dong, Y. Hu, C. Zhou, S. Zhang, Y. Zhong, S. Liang, L. Zhang, Perturbation-driven echo-like superfluorescence in perovskite superlattices, Adv. Photonics 5 (2023) 055001.
[2] G. Rainò, M.A. Becker, M.I. Bodnarchuk, R.F. Mahrt, M.V. Kovalenko, T. Stöferle, Superfluorescence from lead halide perovskite quantum dot superlattices, Nature 563 (2018) 671–675.
[3] D. Lapkin, C. Kirsch, J. Hiller, D. Andrienko, D. Assalauova, K. Braun, J. Carnis, Y. Y. Kim, M. Mandal, A. Maier, Spatially resolved fluorescence of caesium lead halide perovskite supercrystals reveals quasi-atomic behavior of nanocrystals, Nat. Commun. 13 (2022) 892.
[4] Y. Li, F. Zhang, Self-assembly of perovskite nanocrystals: from driving forces to applications, J. Energy Chem. 88 (2023) 561–578.
[5] G. Findik, M. Biliroglu, D. Seyitliyev, J. Mendes, A. Barrette, H. Ardekani, L. Lei, Q. Dong, F. So, K. Gundogdu, High-temperature superfluorescence in methyl ammonium lead iodide, Nat. Photonics 15 (2021) 676–680.
[6] C. Zhou, Y. Zhong, H. Dong, W. Zheng, J. Tan, Q. Jie, A. Pan, L. Zhang, W. Xie, Cooperative excitonic quantum ensemble in perovskite-assembly superlattice microcavities, Nat. Commun. 11 (2020) 329.
[7] Z. Liu, X. Qin, Q. Chen, T. Jiang, Q. Chen, X. Liu, Metal–halide perovskite nanocrystal superlattice: self-assembly and optical fingerprints, Adv. Mater. 35 (2023) 2209279.
[8] H. Pashaei Adl, S. Gorji, G. Muñoz-Matutano, A.F. Gualdrón-Reyes, I. Suárez, V. S. Chirvony, I. Mora-Seró, J.P. Martínez-Pastor, Superradiance emission and its thermal decoherence in lead halide perovskites superlattices, Adv. Opt. Mater. 11 (2023) 2202497.
[9] A. Zhizhchenko, S. Syubaev, A. Berestennikov, A.V. Yulin, A. Porfirev, A. Pushkarev, I. Shishkin, K. Golokhvast, A.A. Bogdanov, A.A. Zakhidov, Single-mode lasing from imprinted halide-perovskite microdisks, ACS Nano 13 (2019) 4140–4147.
[10] E. Tiguntseva, K. Koshelev, A. Furasova, P. Tonkaev, V. Mikhailovskii, E. V. Ushakova, D.G. Baranov, T. Shegai, A.A. Zakhidov, Y. Kivshar, Room-temperature lasing from Mie-resonant nonplasmonic nanoparticles, ACS Nano 14 (2020) 8149–8156.
[11] E.Y. Tiguntseva, D.G. Baranov, A.P. Pushkarev, B. Munkhbat, F. Komissarenko, M. Franckevicius, A.A. Zakhidov, T. Shegai, Y.S. Kivshar, S.V. Makarov, Tunable hybrid Fano resonances in halide perovskite nanoparticles, Nano Lett. 18 (2018) 5522–5529.

[12] A.S. Berestennikov, P.M. Voroshilov, S.V. Makarov, Y.S. Kivshar, Active meta-optics and nanophotonics with halide perovskites, Appl. Phys. Rev. 6 (2019).
[13] Q. Zhang, R. Su, X. Liu, J. Xing, T.C. Sum, Q. Xiong, High-quality whispering-gallery-mode lasing from cesium lead halide perovskite nanoplatelets, Adv. Funct. Mater. 26 (2016) 6238–6245.
[14] J. Song, Q. Shang, X. Deng, Y. Liang, C. Li, X. Liu, Q. Xiong, Q. Zhang, Continuous-wave pumped perovskite lasers with device area below 1 μm^2, Adv. Mater. 35 (2023) 2302170.
[15] B. Tang, H. Dong, L. Sun, W. Zheng, Q. Wang, F. Sun, X. Jiang, A. Pan, L. Zhang, Single-mode lasers based on cesium lead halide perovskite submicron spheres, ACS Nano 11 (2017) 10681–10688.
[16] C. Zhou, J.M. Pina, T. Zhu, D.H. Parmar, H. Chang, J. Yu, F. Yuan, G. Bappi, Y. Hou, X. Zheng, Quantum dot self-assembly enables low-threshold lasing, Adv. Sci. 8 (2021) 2101125.
[17] J. Xu, C.C. Boyd, Z.J. Yu, A.F. Palmstrom, D.J. Witter, B.W. Larson, R.M. France, J. Werner, S.P. Harvey, E.J. Wolf, W. Weigand, S. Manzoor, M.F.A.M. Hest, J. J. Berry, J.M. Luther, Z.C. Holman, M.D. Mcgehee, Triple-halide wide–band gap perovskites with suppressed phase segregation for efficient tandems, Science 367 (2020) 1097–1104.
[18] W. Mao, C.R. Hall, S. Bernardi, Y.B. Cheng, A. Widmer-Cooper, T.A. Smith, U. Bach, Light-induced reversal of ion segregation in mixed-halide perovskites, Nat. Mater. 20 (2021) 55–61.
[19] D.J. Slotcavage, H.I. Karunadasa, M.D. McGehee, Light-induced phase segregation in halide-perovskite absorbers, ACS Energy Lett. 1 (2016) 1199–1205.
[20] Y. Mi, Y. Zhong, Q. Zhang, X. Liu, Continuous-wave pumped perovskite lasers, Adv. Opt. Mater. 7 (2019) 1900544.
[21] F. Zhao, A. Ren, P. Li, Y. Li, J. Wu, Z.M. Wang, Toward continuous-wave pumped metal halide perovskite lasers: strategies and challenges, ACS Nano 16 (2022) 7116–7143.
[22] D. Han, M. Imran, M. Zhang, S. Chang, X. g. Wu, X. Zhang, J. Tang, M. Wang, S. Ali, X. Li, Efficient light-emitting diodes based on in situ fabricated $FAPbBr_3$ nanocrystals: the enhancing role of the ligand-assisted reprecipitation process, ACS Nano, 12 (2018) 8808-8816.
[23] Q.A. Akkerman, G. Rainò, M.V. Kovalenko, L. Manna, Genesis, challenges and opportunities for colloidal lead halide perovskite nanocrystals, Nat. Mater. 17 (2018) 394–405.
[24] D. Yang, X. Zhang, Y. Yang, Z. Xu, S. Liu, K. Cheng, S. Guo, Q. Xu, S. Jeon, L. Li, Revealing the self-assembly behavior of CsPbBr 3 nanoscale supercrystals mediated by packed clusters, ACS Mater. Lett. 6 (2024) 1439–1446.
[25] Y. Zhong, C. Zhou, L. Hou, J. Li, W. Xie, H. Dong, L. Zhang, Ultrafast optical properties of cavity-enhanced superfluorescence, Adv. Opt. Mater. 10 (2022) 2102290.
[26] J. Liu, X. Zheng, O.F. Mohammed, O.M. Bakr, Self-assembly and regrowth of metal halide perovskite nanocrystals for optoelectronic applications, Acc. Chem. Res. 55 (2022) 262–274.
[27] H. Huang, M.W. Feil, S. Fuchs, T. Debnath, A.F. Richter, Y. Tong, L. Wu, Y. Wang, M. Döblinger, B. Nickel, Growth of perovskite CsPbBr 3 nanocrystals and their formed superstructures revealed by in situ spectroscopy, Chem. Mater. 32 (2020) 8877–8884.
[28] T. Hu, D. Li, Q. Shan, Y. Dong, H. Xiang, W.C. Choy, H. Zeng, Defect behaviors in perovskite light-emitting diodes, ACS Mater. Lett. 3 (2021) 1702–1728.
[29] E. Oksenberg, A. Merdasa, L. Houben, I. Kaplan-Ashiri, A. Rothman, I. G. Scheblykin, E.L. Unger, E. Joselevich, Large lattice distortions and size-dependent bandgap modulation in epitaxial halide perovskite nanowires, Nat. Commun. 11 (2020) 489.
[30] B. Zhang, D. Altamura, R. Caliandro, C. Giannini, L. Peng, L. De Trizio, L. Manna, Stable CsPbBr 3 nanoclusters feature a disk-like shape and a distorted orthorhombic structure, J. Am. Chem. Soc. 144 (2022) 5059–5066.
[31] W. Zhuang, S. Li, F. Deng, G. Li, S. Tie, S. Lan, Laser writing of CsPbBr 3 nanocrystals mediated by closely-packed Au nanoislands, Appl. Surf. Sci. 538 (2021) 148143.
[32] S. Li, M. Yuan, W. Zhuang, X. Zhao, S. Tie, J. Xiang, S. Lan, Optically-controlled quantum size effect in a hybrid nanocavity composed of a perovskite nanoparticle and a thin gold film, Laser Photonics Rev. 15 (2021) 2000480.
[33] S. Sun, Z. Cheng, J. Song, C. Yan, T. Man, G. Dong, B. Qian, J. Qiu, Low-power-consumption, reversible 3D optical storage based on selectively laser-induced photoluminescence degradation in CsPbBr 3 quantum dots doped glass, Adv. Mater. Technol. 7 (2022) 2200470.
[34] J. Shi, W. Ge, Y. Tian, M. Xu, W. Gao, Y. Wu, Enhanced stability of all-inorganic perovskite light-emitting diodes by a facile liquid annealing strategy, Small 17 (2021) 2006568.
[35] S.Y. Liang, H.J. Zhang, Y.F. Liu, Z.K. Ji, H. Xia, H.B. Sun, High-resolution in situ crystallization and patterning of a CsPbBr 3 film via femtosecond laser printing, ACS Photonics 10 (2023) 3188–3194.
[36] P. Vashishtha, I.H. Abidi, S.P. Giridhar, A.K. Verma, P. Prajapat, A. Bhoriya, B. J. Murdoch, J.O. Tollerud, C. Xu, J.A. Davis, CVD-grown monolayer MoS_2 and GaN thin film heterostructure for a self-powered and bidirectional photodetector with an wxtended active spectrum, ACS Appl. Mater. Interfaces 16 (2024) 31294–31303.
[37] P. Vashishtha, A. Dash, P. Prajapat, P. Goswami, S. Walia, G. Gupta, Self-powered broadband photodetection of MoS_2/Sb_2Se_3 heterostructure, ACS Appl. Opt. Mater. 1 (2023) 1952–1962.
[38] P. Vashishtha, S.K. Jain, P. Prajapat, A.K. Verma, N. Aggarwal, B.J. Murdoch, S. Walia, G. Gupta, A Self-driven bidirectional photocurrent photodetector for optically controlled logic gates utilizes a GaN-nanowall network, ACS Appl, Opt. Mater. (2024).
[39] H. Huang, F. Deng, J. Xiang, S. Li, S. Lan, Plasmon-exciton coupling in dielectric-metal hybrid nanocavities with an embedded two-dimensional material, Appl. Surf. Sci. 542 (2021) 148660.
[40] J. Xiang, M. Panmai, S. Bai, Y. Ren, G.C. Li, S. Li, J. Liu, J. Li, M. Zeng, J. She, Y. Xu, S. Lan, Crystalline silicon white light sources driven by optical resonances, Nano Lett. 21 (2021) 2397–2405.
[41] Z. Lin, R. Huang, S. Li, S. Liu, J. Song, M. Panmai, S. Lan, Ultralow threshold lasing from a continuous-wave-pumped SiN_x/CsPbBr 3/Ag thin film mediated by the whispering gallery modes of a Si_O2 microsphere, J. Phys. Chem. Lett. 13 (2022) 9967–9974.
[42] P. Vashishtha, A. Dash, K. Kumar, P. Prajapat, M. Kumar, S. Walia, G. Gupta, Self-powered, thermally stable Sb_2Se_3-based high-performance broadband photodetector, Opt. Laser Technol. 169 (2024) 110114.
[43] P. Vashishtha, A.K. Verma, S. Walia, G. Gupta, A solar-blind ultraviolet photodetector with self-biasing capability, controlled by surface potential based on GaN hexagonal nano-spikes, Mater. Lett. 136708 (2024).
[44] P. Vashishtha, P. Prajapat, K. Kumar, M. Kumar, S. Walia, G. Gupta, Multiband spectral response inspired by ultra-high responsive thermally stable and self-powered Sb_2Se_3/GaN heterojunction based photodetector, Surf. Interfaces 42 (2023) 103376.
[45] C. Wang, D. Han, J. Wang, Y. Yang, X. Liu, S. Huang, X. Zhang, S. Chang, K. Wu, H. Zhong, Dimension control of in situ fabricated CsPbClBr 2 nanocrystal films toward efficient blue light-emitting diodes, Nat. Commun. 11 (2020) 6428.
[46] P.B. Johnson, R.W. Christy, Optical constants of the noble metals, Phys. Rev. B 6 (1972) 4370.
[47] X. Chen, Y. Wang, J. Song, X. Li, J. Xu, H. Zeng, H. Sun, Temperature dependent reflectance and ellipsometry studies on a CsPbBr 3 single crystal, J. Phys. Chem. C 123 (2019) 10564–10570.
[48] G.A. Elbaz, W.L. Ong, E.A. Doud, P. Kim, D.W. Paley, X. Roy, J.A. Malen, Phonon speed, not scattering, differentiates thermal transport in lead halide perovskites, Nano Lett. 17 (2017) 5734–5739.
[49] T. Haeger, M. Ketterer, J. Bahr, N. Pourdavoud, M. Runkel, R. Heiderhoff, T. Riedl, Thermal properties of $CsPbCl_3$ thin films across phase transitions, J. Phys.-Mater. 3 (2020) 024004.
[50] R. Evarestov, E. Kotomin, A. Senocrate, R. Kremer, J. Maier, First-principles comparative study of perfect and defective $CsPbX_3$ (X= Br, I) crystals, Phys. Chem. Chem. Phys. 22 (2020) 3914–3920.
[51] X. Zhang, P. Yang, $CsPbX_3$ (X= Cl, Br, and I) Nanocrystals in substrates toward stable photoluminescence: Nanoarchitectonics, properties, and applications, Langmuir 39 (2023) 11188–11212.
[52] Y. Tong, E.P. Yao, A. Manzi, E. Bladt, K. Wang, M. Döblinger, S. Bals, P. Müller-Buschbaum, A.S. Urban, L. Polavarapu, Spontaneous self-assembly of perovskite nanocrystals into electronically coupled supercrystals: toward filling the green gap, Adv. Mater. 30 (2018) 1801117.
[53] L. Chen, D. Mao, Y. Hu, H. Dong, Y. Zhong, W. Xie, N. Mou, X. Li, L. Zhang, Stable and ultrafast blue cavity-enhanced superfluorescence in mixed halide perovskites, Adv. Sci. 10 (2023) 2301589.
[54] A. Nicarel, M. Oane, I.N. Mihailescu, C. Ristoscu, Fourier two-temperature model to describe ultrafast laser pulses interaction with metals: A novel mathematical technique, Phys. Lett. A 392 (2021) 127155.
[55] V.E. Alexopoulou, A.P. Markopoulos, An advanced methodology for the development of highly accurate two temperature models (TTMs) to describe the material irradiation by an ultrashort laser, Opt. Laser Technol. 177 (2024) 111062.
[56] R. Gan, H. Fan, Z. Wei, H. Liu, S. Lan, Q. Dai, Photothermal response of hollow gold nanorods under femtosecond laser irradiation, Nanomaterials 9 (2019) 711.
[57] B.H. Christensen, K. Vestentoft, P. Balling, Short-pulse ablation rates and the two-temperature model, Appl. Surf. Sci. 253 (2007) 6347–6352.
[58] S.-A. Anghel, M. Oane, C.N. Mihăilescu, B.A. Sava, M. Elişa, N. Mihăilescu, D. Ticoş, A.M. Trefilov, C. Ristoscu, A.V. Filip, Thermal lattice field during ultra-short laser pulse irradiation of metal targets: a fokker–planck analytical model, Metals 13 (2023) 1775.
[59] Z. Lin, R. Huang, W. Zhang, Y. Zhang, J. Song, H. Li, D. Hou, Y. Guo, C. Song, N. Wan, Highly luminescent and stable Si-based CsPbBr 3 quantum dot thin films prepared by glow discharge plasma with real-time and in situ diagnosis, Adv. Funct. Mater. 28 (2018) 1805214.